2023

Study Protocol to Analyze the Effects of Occupational Exoskeleton Use on Balance Control

Vishnu Sai Prabhakarababu
pvishnusai98@gmail.com

ABSTRACT

STUDY PROTOCOL TO ANALYZE THE EFFECTS OF OCCUPATIONAL EXOSKELETON USE ON BALANCE CONTROL

Vishnu Sai Prabhakarababu, MS
Department of Industrial and Systems Engineering
Northern Illinois University, 2023
Dr. Ting Xia, Co-Director
Dr. Jaejin Hwang, Co-Director

Work-related musculoskeletal disorders (MSDs) represent a prevalent concern affecting a wide range of industries. Occupational exoskeletons have garnered attention as a potential solution to alleviate the risk of MSDs by reducing mechanical loads on susceptible body regions. A critical knowledge gap exists regarding the complex interactions between exoskeleton use and the human body, particularly in work environments prone to slips, trips and falls. This thesis work was part of a funded research aiming to determine the effects of exoskeleton use on balance control. The primary purpose of this thesis work was to determine a reliable maker placement protocol that will be used in the funded research. Two motion data-based approaches were chosen to track full-body kinematics. In the direct center of joint approach (RawJC), paired markers were placed on the opposite sides of major body joints with the midpoints serving as joint centers. The centers of mass (CoM) was then derived from the proximal and distal joint centers of segments and further the whole-body CoM. In the skeletal model-based approach, a skeletal model paired with the conventional full-body, 39-marker placement protocol was used to predict the joint centers, the segmental CoM, and the whole-body CoM. During testing, the

participants were asked to perform 3 tasks during quiet standing and during walking. The tasks were 1) holding a weight carrying posture with empty hands, 2) carrying weight (7.0 kg) in the hands, and 3) carrying weight in the hands while wearing a mock exoskeleton (10.3 kg). The two approaches were tested in a single setup by placing all necessary markers on the body. The whole-body CoM was calculated in 4 ways: 1) RawJC – using direct measures of joint centers, the Dempster segmentation method, and the segmental masses from Webb Associates, 2) ModelJC – using the model-produced joint centers, the Dempster segmentation method, and the segmental masses from Webb Associates, 3) ModelCoM – using the model-produced segmental CoM and the segmental masses from Webb Associates, and 3) ModelWBCoM – using the model-produced whole-body CoM. During quiet standing, all four motion data-based methods were compared to the center of pressure (FPCoP) obtained using a force plate placed under the participant's feet. The results showed that the FPCoP was posterior to the RawJC-derived CoM, which was in turn posterior to the 3 model-derived CoM. In the side-to-side direction, the FPCoP located at the middle while the 4 motion data-based CoM were slightly to the left side. The anterior-posterior sway distance, the side-to-side sway distance and the sway speed analyses showed no difference between the 4 motion data-based methods. The task effect analyses showed that wearing the mock exoskeleton caused the CoM to shift a higher position. Also, carrying weight in hands and carrying weight while wearing an exoskeleton caused CoM to shift posteriorly. Both observations on the task effect indicate potentially compromised balance ability. During walking, the analyses of the CoM computing method effect showed that the RawJC and ModelWBCoM methods were similar while the ModelJC and ModelCoM were similar. Together, the data collected in this thesis work suggest that both the RawJC and

ModelWBCoM were suitable to study the risk of falls during slips and falls, with a slight preference to the RawJC method due to its simplicity.

NORTHERN ILLINOIS UNIVERSITY
DEKALB, ILLINOIS

DECEMBER 2023

STUDY PROTOCOL TO ANALYZE THE EFFECTS OF OCCUPATION EXOSKELETON USE ON BALANCE CONTROL

BY

VISHNU SAI PRABHAKARABABU

A THESIS SUBMITTED TO THE GRADUATE SCHOOL

IN PARTIAL FULFILLMENT OF THE REQUIREMENTS

FOR THE DEGREE

MASTER OF SCIENCE

DEPARTMENT OF INDUSTRIAL AND SYSTEMS ENGINEERING

Thesis Co-Director:
Dr. Ting Xia

Thesis Co-Director:
Dr. Jaejin Hwang

ACKNOWLEDGEMENTS

I would like to express my heartfelt gratitude to Northern Illinois University and the Department of Industrial and Systems Engineering for their unwavering support and encouragement throughout my academic journey, from the very beginning to its conclusion. I would like to extend my sincere appreciation to NIU Great Journeys for its invaluable assistance in funding my research. A special acknowledgment and deep appreciation go to my thesis advisor, Dr. Ting Xia, whose guidance, wealth of expertise, unwavering dedication, and boundless energy have played a pivotal role in nurturing my growth within this research field. I am grateful to Dr. Jaejin Hwang, who served as both my academic advisor and co-advisor for my thesis. His unwavering support and expert guidance were instrumental throughout the entire thesis process. I extend my sincere thanks and appreciation to Dr. Ziteng Wang, a member of my committee, for providing invaluable feedback and words of encouragement. I feel fortunate to have collaborated with Dr. Ram Haddas, another esteemed committee member, whose insightful feedback greatly contributed to the quality of my thesis work. Special appreciation goes to my professor in Industrial and Systems Engineering, Dr. Purushothaman Damodaran, who has not only been a great mentor in my academic journey but also a significant influence on my career. Lastly, I would like to express my gratitude to my dear friend Vishal Garela for his unwavering support and motivation.

DEDICATION

I want to express my heartfelt appreciation to my loving family, whose unwavering dedication and unconditional support have been the pillars of my life. My dear father, Prabhakarababu, has been a constant source of inspiration and faith in me, while my mother, Jayalakshmi, has provided caring and warm encouragement. I extend my gratitude to my sister, Dr. P Seelabanu, and my brother-in-law, Dr. P Bharath Kumar, for their steadfast support throughout my life journey. I also want to acknowledge the incredible presence of my best friends, Sunil Puli, Shiby Gabrial, Sobhit Pokhrel, Ayaz Niazi and Mobasshira Zaman who have enriched my life with their love, support, concern, and motivating presence. Special mention goes to my cherished friend, Roommate, Vishal Garela, who has consistently been there to support me.

TABLE OF CONTENTS

Page

Page

LIST OF TABLES

Page

Page

LIST OF FIGURES

Page

Page

CHAPTER 1: INTRODUCTION

1.1 Background

The prevalence of work-related Musculoskeletal Disorders (MSDs) in the industrial landscape remains a persistent challenge. A considerable portion of work-related MSD have been linked to the excessive and repetitive physical strains encountered in the workplace. The gravity of the issue is highlighted by a recent survey conducted by the US Bureau of Labor Statistics that within the private sector in 2018, a total of 272,780 cases of MSDs were reported (U.S. Bureau of Labor Statistics, 2018, p. 2). The risk of MSDs is increased by the duration of work, the weight of the load being lifted, and the awkward posture (Anderson, 1984). Strategies for mitigating these risks include load reduction using assistive devices, modification of arm postures, elevation of body positions, and limitation of exposure time.

In the past few decades, there has been a notable increase in the interest surrounding occupational exoskeletons due to their potential to improve efficiency, increase productivity, and reduce the occurrence of injuries. The manufacturing industries has been leading the way of integration of exoskeleton in the workplace. Boeing, for instance, has implemented approximately 100 passive upper-extremity exoskeletons across various locations within the United States. Toyota Motor North America mandates the use of exoskeletons for 500 workers, aiming to enhance workforce ergonomics. Despite the increasing adoption of exoskeletons, the lack of standardized guidelines hindered both designers and consumers in the evaluation and selection processes. This lack of standardized protocols, as noted by Lowe et al. (2019), is a result of the varying effects of occupational exoskeletons on the physical burden of the upper

extremities, especially during overhead activity (Kudernatsch and Peterson, 2018; Kim et al., 2018).

Besides the understanding of the benefits of using occupational exoskeletons in the workplace, there also needs a good understand of associated risks. Particularly for the funded research that this thesis work is to support, it aims to determine the impact of occupational exoskeleton use on balance control. Very limited literature data are available to address this issue especially at the workplace prone to slips and trips such as fishing industries. Overall, the adoption rate in industries is outpacing our understanding of benefits and risks associated with occupational exoskeleton use in the highly varying work environments.

1.2 Objectives

The incorporation of occupational exoskeletons into modern workplaces has emerged as a promising option to improve worker performance and decrease the risks associated with performing physically demanding activities. However, there is a major knowledge gap about potential hazards associated with the use of occupational exoskeletons, in working environments that are prone to slips, trips, and falls. These risks include a variety of different aspects, such as the potential for disruption of balance due to the increased weight of the exoskeleton itself, the counteractive forces applied by the exoskeleton onto the body of the wearer, and the imposition of limitations on the wearer's range of motion due to the design of the exoskeleton.

This thesis work was part of a funded research aiming to investigate the effects of exoskeleton use on balance control. Particularly, the purpose of this thesis work was to determine a reliable maker placement protocol that will be used in the funded research to study exoskeleton-assisted weight carrying tasks and risk of falls. The main goal of this thesis work

was to compare two motion capture approaches that are used to track the kinematics of individual body segments in order to compute the whole-body center of mass (CoM) when the participants were standing still and walking. The results of this study will provide evidence to choose the best marker protocol for the funded research that required precise and accurate motion capture and CoM computation during slips and falls.

CHAPTER 2: LITERATURE REVIEW

2.1 Marker Placement Protocol Used in Tracking Full-Body Kinematics

Haddas & Lieberman (2017) has done some functional balance tests to evaluate postural control and to identify the balance deficits in individuals with special conditions, such as Adolescent Idiopathic Scoliosis (AIS). Each subject was equipped with 51 external reflective markers placed strategically on anatomical landmarks. Haddas et al. (2020) also explores the methodological aspects of dynamic balance testing with a focus on marker-based kinematic analysis and marker placement. Subjects were equipped with a full body marker set comprising 41 external reflective markers strategically placed on anatomical landmarks. These markers included those overlying the C7 and T12 spinous processes, jugular notch, xiphoid process, right scapula, and multiple points on the upper and lower extremities.

Rakshit et al. (2020) conducted a study involving 19 participants to investigate various aspects of weightlifting experiments. In their study, Rakshit et al. (2020) employed a marker protocol that utilized a plug-in-gait model with added iliac crests, resulting in a total of 42 markers placed strategically on the participants' bodies. The placement of these markers was a critical step in capturing accurate kinematic data during weightlifting tasks. Haddas et al. (2021) conducted a study focusing on patients with degenerative spinal pathologies to assess their balance control and dynamic compensatory mechanisms before surgical intervention. Each patient was equipped with a full-body external reflective marker set for three-dimensional (3D) balance analysis, with markers strategically placed to track primary joints of the trunk and extremities. Haddas et al. (2021) conducted an experiment focusing on the relationship between

the Cone of Economy (CoE) and the Center of Pressure (CoP) in patients with spine pathologies and healthy controls. To enable the collection of three-dimensional kinematic data, each participant was fitted with fifty reflective markers.

Haddas et al. (2019) conducted an extensive study involving both kinematic and electromyographic (EMG) data collection to gain insights into postural control and musculoskeletal activity. All test subjects were equipped with a full-body marker set, consisting of 50 external reflective markers placed strategically on anatomical landmarks. These markers were meticulously positioned on the skin overlying key points, including spinous processes, the scapula, head, and various upper and lower limb segments. Triad markers were also placed on the cervical and lumbar vertebrae to record spine kinematics. Anthropometric measurements, such as height, weight, pelvic width, extremity lengths, and major joint width, were taken to account for individual variations in body proportions.

Haddas et al. (2019) conducted a comprehensive study that integrated detailed anthropometric measurements and advanced kinematic data collection techniques to gain insights into functional balance tests. All test subjects were fitted with a set of 41 external reflective markers strategically positioned on anatomical landmarks, encompassing the T10 and C7 spinous processes, sternal notch, xiphoid process, right scapula, and bilateral placements on key anatomical points, including the upper extremities, trunk, head, and lower extremities. This marker set allowed for precise tracking of body segments during functional balance tests.

In a recent study conducted by Grooten et al. (2022), a comprehensive investigation into the biomechanics of lifting tasks on surfaces with varying degrees of instability was carried out. Data collection for this study was conducted using an optical motion capture system (Vicon, Oxford Metrics, UK) equipped with 28 markers attached directly to the participants' bodies using

double-sided tape and a headband. Additionally, an extra marker was affixed to the back of the box to track its movements.

(Burkhart et al., 2020) applied optoelectronic motion capture data to investigate the evaluation of inter-session reliability in the construction of musculoskeletal models that are specific to each subject. The identification of anatomical landmarks involved manual palpation, followed by the affixation of retroreflective markers to the skin using double-adhesive tape. Rigid clusters, each comprising four markers, were securely fastened over the palpated spinous processes at T1, T4, T5, T8, T9, T12, and L1. Additional markers were strategically positioned at key anatomical landmarks on the pelvis, encompassing the posterior (PSIS) and anterior (ASIS) superior iliac spines, as well as the iliac crests. Further markers were placed at C7, in addition to bilateral markers affixed to the acromion (shoulder), lateral epicondyle of the humerus (elbow), radial styloid process (wrist), greater trochanter of the femur, lateral and medial aspects of the knee joint, lateral and medial aspects of the ankle joint, posterior heel, and the first metatarsophalangeal (MTP) joint (big toe). Head motion was tracked using a headband equipped with four markers, while an additional 41 markers were situated on the sternum, clavicles, and extremities (Burkhart et al., 2020).

Haddas & Lieberman (2017) involved ten AIS patients and ten non-scoliotic volunteers; a comprehensive approach was employed to investigate functional balance. Three-dimensional (3D) kinematic data were meticulously recorded at a high sampling rate of 100 Hz using a sophisticated 10-camera Vicon Video system (Vicon Nexus 2.7 Inc., Englewood, CO, USA), as described by Haddas & Lieberman (2017). Furthermore, simultaneous EMG data were captured at a rate of 2000 Hz, allowing for a comprehensive assessment of neuromuscular responses

during the balance tests. To ensure data quality, the kinematic data underwent low-pass filtering with a fourth-order Butterworth filter, with a lower cutoff at 4 Hz.

Rakshit et al.'s (2020) utilized two force plates—one under each of the participants' feet—to collect ground reaction forces (GRF) at a high sampling rate of 2000 Hz. The GRF data provide valuable insights into the biomechanics of weightlifting movements. The marker-labeled data collected during the experiment were subjected to data smoothing and converted into a C3D file format. Subsequently, this data was imported into Visual 3D software for further analysis. Haddas et al. (2021) conducted a study focusing on patients with degenerative spinal pathologies, in this study, they acquired three-dimensional (3D) kinematic data at a high sampling rate of 100 Hz using a 10-camera system and subsequent low-pass filtering were integral steps in ensuring the accuracy of balance measurements. Statistical analysis, conducted using one-way ANOVAs, compared the degenerative spinal pathology cohorts to the healthy group, unveiling significant differences that can inform preoperative assessments.

Haddas et al. (2021) conducted an experiment focusing on the relationship between the Cone of Economy (CoE), in this experiment, CoE kinematics were recorded at a sampling rate of 100 Hz using Vicon Nexus 2.0 Inc., Englewood, CO. CoP data were collected concurrently at 2000 Hz using a single force plate from AMTI, Watertown, MA. A standing static trial was conducted to establish a reference position for defining neutral joint angles.

The raw data collected from the Vicon video system and force plate were processed using a custom laboratory algorithm implemented in MATLAB. Raw 3D coordinate data underwent smoothing through a fourth order no-phase-shift Butterworth low-pass digital filter with a cutoff frequency set at 4 Hz. This preprocessing step was essential to enhance data quality before further analysis.

2.2 Segmentation Methods and Determination of Center of Mass

Dempster's method is a widely recognized approach to segmenting the human body. Dempster's method divides the body into a larger number of segments, with a focus on anatomical precision. Segments in Dempster's method include head, neck, trunk, upper arm, forearm, hand, thigh, shank, foot (Dempster, 1955). Dempster gathered information from eight cadavers, he segmented the cadavers according to his own method, and then carefully documented the lengths, masses, and volumes. Dempster created a table where he showed the mass of a segment as a ratio of the mass of that segment to the total body mass. He presented the length of the segments as a proportion of length of the COM and the total segmental length. These data in the modified form are shown in Table 2.1 (Miller and Nelson, 1973; Plagenhoef 1971; Winter 1990).

Table 2.1 Dempster's Body Segment Parameters

Segment	**Endpoints (Proximal to Distal)**	**Segmental Mass/Total Mass**	**Center of Mass/Segment Length**		**Radius of Gyration/Segment Length**		
		(P)[b]	**($R_{proximal}$)[c]**	**(R_{distal})[c]**	**(K_{cg})[d]**	**($K_{proximal}$)[d]**	**(K_{distal})[d]**
Hand	Wrist center to knuckle II of third finger	0.0060	0.506	0.494	0.298	0.587	0.577
Forearm	Elbow to Wrist Center	0.0160	0.430	0.570	0.303	0.526	0.647
Upper arm	Glenohumeral Joint to Elbow Center	0.0280	0.436	0.564	0.322	0.542	0.645
Forearm and hand	Elbow to Wrist Center	0.022	0.682	0.318	0.468	0.827	0.565

(Continued on following page)

Table 2.1 continued

Upper extremity	Glenohumeral Joint to Wrist Center	0.05	0.53	0.470	0.368	0.645	0.596
Foot	Ankle to Ball of Foot	0.0145	0.500	0.500	0.475	0.690	0.690
Leg	Knee to Ankle Center	0.0465	0.433	0.567	0.302	0.528	0.643
Thigh	Hip to Knee Center	0.100	0.433	0.567	0.323	0.540	0.653
Lower Extremity	Hip to Ankle Center	0.1610	0.447	0.553	0.326	0.560	0.650
Head	C7-T1 to ear Canal	0.0810	1.000	0.000	0.495	1.116	0.495
Shoulder	Sternoclavicular Joint to Glenohumeral Joint Center	0.0158	0.712	0.288			
Thorax	C7-T1 to T12-L1	0.2160	0.820	0.180			
Abdomen	T12-L1 to L4-L5	0.1390	0.440	0.560			
Pelvis	L4-L5 to Trochanter	0.1420	0.105	0.895			
Thorax and Abdomen	C7-T1 to L4-L5	0.355	0.630	0.370			
Abdomen and Pelvis	T12-L1 to Greater Trochanter	0.2810	0.270	0.730			
Trunk	Greater Trochanter to Glenohumeral Joint	0.4970	0.495	0.505	0.406	0.640	0.648
Head, Arms, and Trunk	Greater Trochanter to Glenohumeral Joint	0.6780	0.626	0.374	0.496	0.640	0.648
Head, Arms and Trunk	Greater Trochanter to Mid-rib	0.6780	1.142	-0.142	0.903	1.456	0.914

[a]End points; [b]A segments's mass as a proportion of the total body mass; [c]The distances from the proximal and distal ends of the segment to the segment's center of gravity as proportions of the segment's length; [d]The radii of gyration about the center of gravity, proximal and distal ends of the segment to the segment's center of gravity as proportions of the segment's length.

In order to develop a reference model, Webb Associates gathered information regarding the average mass of various body parts (Webb Associates, 1978). This framework develops an essential understanding of the distribution of mass across varying parts of the human body. Table 2.2. shows the segments and associated masses that were used in this thesis work.

Table 2.2 Segmental masses used in this thesis work (adapted from Webb's Associates, 1978).

Segment / Whole-Body Mass	45.73	54.45	63.52	72.59	81.67	90.74
Head	3.87	4.12	4.40	4.68	4.95	5.23
Neck and Torso	21.06	26.13	31.19	36.26	41.33	46.39
Pelvis	5.01	6.26	7.50	8.75	10.00	11.25
Head, Neck, and Torso	24.75	30.14	35.53	40.92	46.31	51.70
Upper arm	1.23	1.48	1.73	1.98	2.23	2.48
Forearm	0.70	0.87	1.04	1.22	1.39	1.56
Hand	0.32	0.37	0.42	0.47	0.52	0.57
Thigh	4.24	5.29	6.34	7.39	8.45	9.50
Shank	2.08	2.42	2.76	3.11	3.45	3.79
Foot	0.78	0.85	0.91	0.97	1.03	1.10

In order to develop a reference model, Webb Associates gathered information regarding the average mass of various body parts (Webb Associates, 1978). This framework develops an essential understanding of the distribution of mass and weight across every part of the human body as shown in Figure 2.

Rakshit et al. (2020) experimentally utilized measured heights and weights of the 19 participants. This information was employed to generate individual body segment lengths,

centers of mass, and inertial properties using GEBOD, a regression-based interactive utility. Generator of Body Data (GEBOD) is used to generate human data sets (Cheng et al., 1994). The data sets include the geometric and mass properties of the body segments, as well as the locations and mechanical properties of the joints. These data sets are computed using regression equations derived from anthropometric surveys and stereo photometric data. In GEBOD, there are four groups of regression equations which are used to determine the body dimension set, joint location coordinates, segment volumes, and principal moments of inertia. Each group has two sets of equations for female and male subjects respectively. Each regression equation is a first order linear equation with either standing height or body weight, or both as independent variables. For example, the regression equation to predict adult female shoulder height can be found as follows:

Shoulder Height - 0.07182(Body Weight) + 42.77

Shoulder Height - 0.8751 (Standing Height) - 3.936

Shoulder Height - 0.00755 (Body Weight) + 0.8469 (Standing Height) - 3.096

where the body weight and standing height are the input variables which the user supplied. Depending on the user input, one of the above three equations is used to obtain the shoulder height. The R2 values for the above three equations are 0.3094, 0.9194 and 0.9218, respectively. As expected, the equation using both weight and height has the best predictive ability (Cheng et al., 1994).

Haddas & Lieberman (2017) conducted some balance tests, the CoM in this experiment was calculated using anthropometric measurements, applying the body segment method and a custom algorithm software that combined Vicon Nexus and MATLAB R2016. Haddas et al. (2020) used one-way ANOVA to find out how the Cone of Economy (CoE) factors and balance

control strategies of ADS patients before surgery were different from those of controls who didn't have scoliosis. 0.05 was chosen as the critical alpha number. SPSS, Version 23.0 (IBM, Inc., Chicago, IL) was used to do the statistical analysis. Haddas et al. (2021) employed anthropometric measurements and a custom software algorithm to determine the CoM, thus addressing the inherent biases associated with conventional BMI calculations.

Haddas et al. (2021) employed Pearson product-moment correlations to explore intercorrelations among CoE and CoP variables, both for spine patients and healthy controls. Once the relationships between these variables were established, linear multiple regression analyses were conducted to predict CoE measurements based on CoP variables. Different combinations of CoP independent variables were entered into models to predict specific CoE variables. These analyses were conducted using SPSS, Version 26.0 (IBM, Armonk, NY, USA).

The calculation of sway was based on established balance work, with the Center of Mass (COM) calculated using anthropometric measurements and custom algorithm software Haddas et al. (2019). The study delved further into postural control by establishing Center of Economy (COE) boundaries, measuring, and calculating COM displacement (middle COE ring) and C7 marker displacement (top COE ring) in both sagittal and coronal planes during the functional balance test.

Haddas et al. (2019) collected all the raw data during the functional balance tests were processed using a custom laboratory algorithm implemented in MATLAB, highlighting the meticulous data analysis process. Center of mass (CoM) calculations was based on anthropometric measurements using the body segment method, facilitated by custom software algorithms.

Burkhart et al. (2020) experimented with a 10-camera motion analysis system (Vicon

Motion Systems, Oxford, UK) helped them keep their bodies in a normal straight standing position while the data was being collected. Explicit instructions were provided, directing subjects to stand upright, distribute their weight evenly on two force plates, and maintain their arms by their sides. Complementary virtual markers and joint centers were derived from the existing set of measured marker data. Hip joint centers, in conjunction with intervertebral joints spanning from C7/T1 to L5/S1, were estimated using established techniques. The knee and ankle joint centers were determined as the midpoint between the medial and lateral joint landmarks. Notably, a central 'head' marker was approximated as the centroid of the four external headband markers. Lastly, markers signifying midPSIS and mid-hip joint centers were established as the midpoint between these preexisting markers.

CHAPTER 3: METHODOLOGY

3.1 Methods in tracking kinematics of body segments

This thesis work seeks to provide methodological support for a funded research aiming to determine the effect of exoskeleton use on balance control, as measured by the risk of falls during various manual handling tasks. Particularly, this thesis work examined two distinct maker placement approaches to monitor the kinematics of body segments, thereby determining the trajectory of the whole-body CoM. The two approaches are 1) Direct center of joint approach and 2) Skeletal model approach.

3.1.1 Direct Center of Joint Approach

In this approach, the human body was divided into 13 segments according to the Dempster segmentation method (1955), including the head/neck/trunk (HNT) segment and the right and left upper arm, forearm, hand, thigh, shank, and foot segments (Figure 3.1). The locations of CoM for these segments are based on the proximal and the distal ends of the segments (Figure 3.1). For example, the upper arm segment is determined by the shoulder joint (the proximal end) and the elbow joint (the distal end) with the CoM located at 43.6% of the segment length from the shoulder joint.

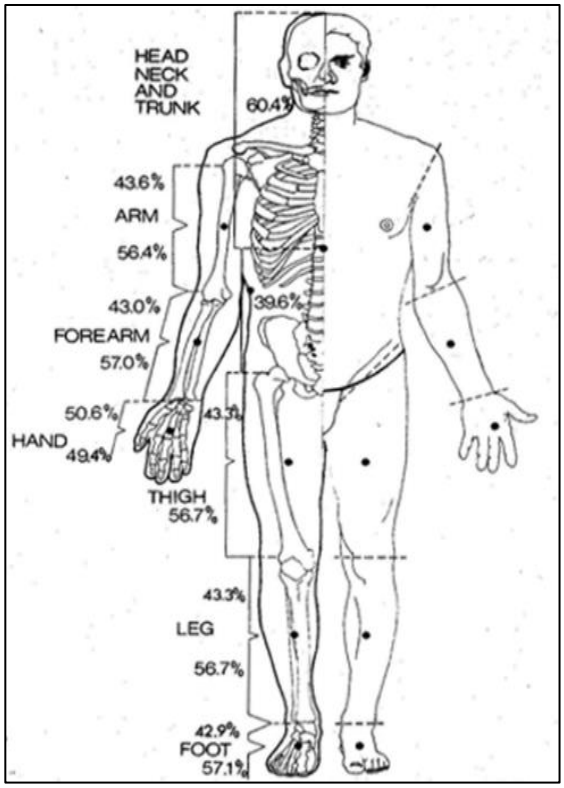

Figure 3.1 Illustration of 13 body segments used in the direct center of joint approach and the locations of the center of mass for each segment (Dempster, 1955).

To track the center of a target joint (except the hip joints), two reflective markers are placed on both sides of the joint with the midpoint between the two markers serving as the joint center. The right and left hip joints were determined using the two makers (RP and LP) placed on the right and left great trochanters with one quarter distance from the respective markers as the joint centers (O'Connor, 2010, Sinclair et al., 2014). Table 3.1 describes the placement of the paired markers at individual joints. The asterisk (*) signs denote the markers not shared with the conventional full-body 39 marker placement protocol. Special cares were needed to determined the CoMs for the HNT segment, the hand segment and the foot segment. The HNT segment does

not have the priximal joint center explicitly defined using markers. Instead, the CoM of the HNT segment is cacluated from the distal end defined by the midpoint (the MidHip landmark) of the RP and LP markers. The CoM location was assumed to be aligned in the vertical direction from the MidHip lardmark during the T-Pose. The relationship between the HNT CoM and the thorax (i.e., the rigid body defined by the C7, clavicle and sternum markers) was determined in the T-Pose and subsequently was used to track the HNT CoM during testing. For the hand segements, the wrist joint center and the two hand markers (placed at the metacarpophalangeal joints of the index and pinky fingers) formed the hand marker plane. The hand CoM was determiend as the midpoint of the two hand markers extended 5 cm ventrically from the hand marker plane to reflect the grabbing posture held by the hands. The foot CoM was determined by the heel marker and the foot tip marker.

Table 3.1 Marker placement at individual body joints and associated anatomic landmarks.

Joint name (left side shown)	**Marker 1**	**Marker 2**
Shoulder	LSF *	LSB *
Elbow	LELB	LHME *
Wrist	LWRB	LWRA
Hand	LFIN	LHF *
Hip	LP *	RP *
Knee	LKNE	LIKNEE *
Ankle	LANK	LIANKLE *
Foot	LHEE	LFTIP

Note: * - markers not shared with the conventional 39 marker placement protocol; LSF – lesser tuberosity of the left humeral head, LSB – back side of the left humeral head, LELB – left humeral lateral epicondyle, LHME – left humeral medial epicondyle, LWRB – left ulnar styloid process, LWRA – left radial styloid process, LFIN – the metacarpophalangeal joint of the left index finger, LHF – the metacarpophalangeal joint of the left pinky finger, LP – left greater trochanter, RP – right greater trochanter, LKNE – left distal femoral lateral epicondyle, IKNEE –left distal femoral medial epicondyle, LANK – left lateral malleolus, IANKLE – left medial malleolus, LHEE – left foot dorsal calcaneus, and LFTIP – tip of the second toe of the left foot.

Overall, 33 markers (11 pairs of joint markers, 4 pairs on the hands and feet, and 3 markers on the thorax) were used in the direct center of joint approach. After determining the joint centers, the locations of individual body segments were computed based on Figure 3.1. The masses of individual body segments were determined using the work of the Webbs Associates (1978). Specifically, a cubic polynomial interpolation (the spline function in MATLAB) was used to obtain segmental masses based on the body mass of each participant.

3.1.2 The Skeletal Model-based Approach

In this approach, a skeletal model with 15 segments and the associated conventional, full-body 39 marker placement protocol were used to track the whole-body motion (Table 3.2). Compared to the direct center of joint approach, this skeletal model further divides the HNT segment into the head, neck/torso/abdomen, and pelvis segments. The skeletal model was constructed in the Visual3D software platform. Each segment is represented by a proximal end, a distal end, and the center of gravity. Table 3.3 summarizes marker grouping for the conventional full body 39 markers. For example, the acromion, mid upper arm, and the lateral elbow epicondyle markers are grouped for the "upper arm" segment. This grouping technique allows the determination of the segmental proximal and distal ends and the segmental CoM using the grouped markers, mass distribution, segment length, and other segment-specific parameters. The

exact values of segmental length and mass were determined by the height and mass of the subjects, thus allowing individualizable skeletal models.

Table 3.2 Anatomic landmarks used in the conventional full-body, 39 marker placement protocol.

Marker Name (Left Side Shown)	**Anatomic Landmarks**
LFHD	Left Anterior Head
LBHD	Left Posterior Head
C7	Cervical Vertebra C7 Spinal Process
CLAV	Sternum Jugular Notch
STRN	Sternum Xiphoid Process
T10	Thoracic Vertebra T10 Spinal process
RBAK	Right Scapula Apex
LASI	Left Anterior Superior Iliac Spine
LPSI	Left Posterior Superior Iliac Spine
LSHO	Left Clavicle Acromion
LUPA	Left Upper Arm
LELB	Right Humerus Lateral Epicondyle
LFRM	Left Forearm
LWRA	Left Radius Styloid Process
LWRB	Left Ulna Styloid Process
LFIN	Left Hand Second metacarpal
LTHI	Left Thigh
LKNE	Left Femur Lateral Epicondyle
LTIB	Left Tibia
LANK	Left Fibula Ankle Lateral
LTOE	Left Foot Second Metatarsal
LHEE	Left Foot Calcaneus

Table 3.3 Marker grouping in the skeletal model using markers from the conventional full body 39 marker placement protocol. The RBAK marker was not used in the skeletal model.

Segment (left side shown)	**Grouped markers**
Head	LFHD, LBHD, RFHD, RBHD
Neck/Thorax/Abdomen	C7, CLAV, STRN, T10
Pelvis	LASI, RASI, LPSI, RPSI
Upper Arm	LSHO, LUPA, LELB
Forearm	LELB,LFRM, LWRA, LWRB
Hand	LWRA, LWRB, LFIN
Thigh	LASI, LTHI, LKNE
Shank	LKNE, LTIB, LANK
Foot	LTOE, LHEE

Figure 3.2 illustrates the conventional full body 39 marker placement for the skeletal model. Figure 3.3 shows 20 additional markers being placed on the body, among which 14 markers were for the direct center of joint approach and 6 additional markers were added to the feet for the base of support determination (not processed in this thesis work).

Figure 3.2 The conventional full-body 39 marker set.

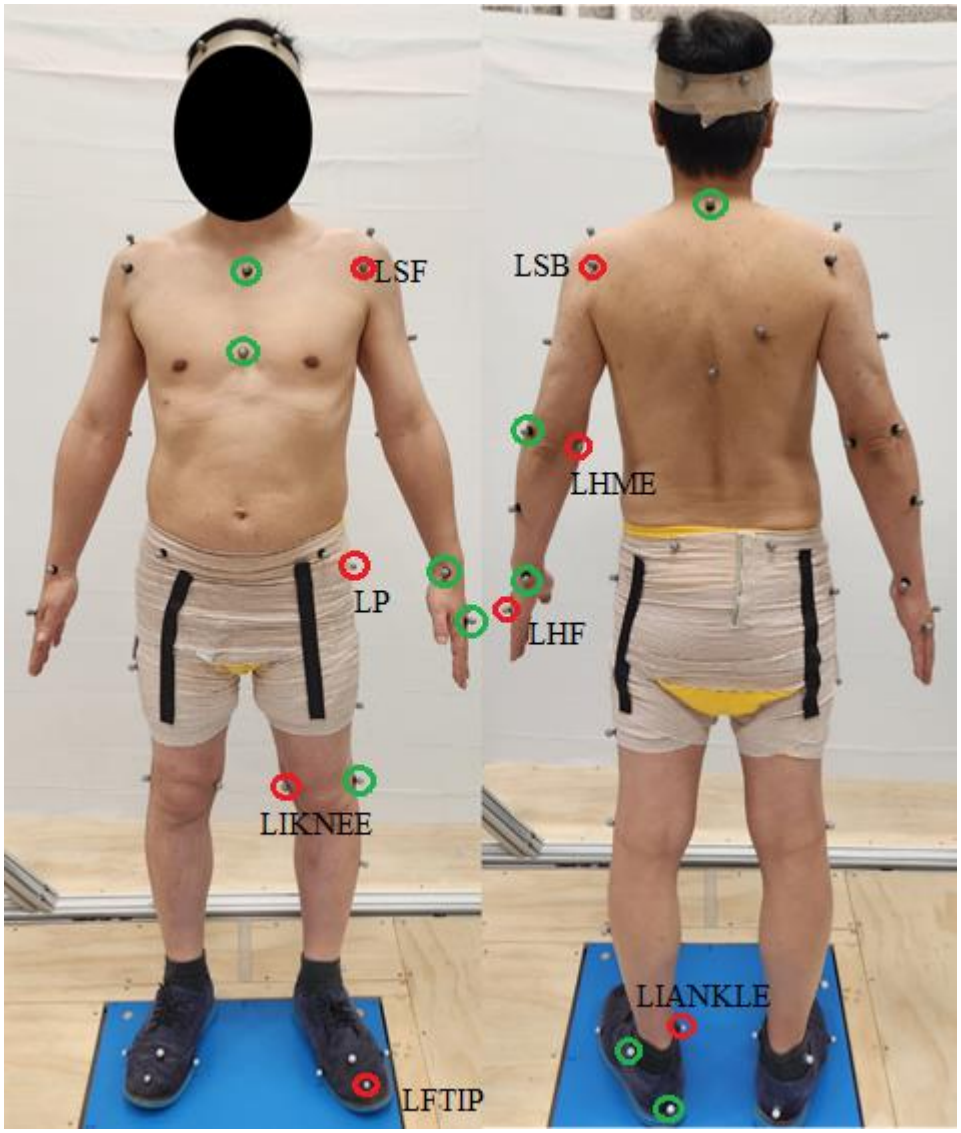

Figure 3.3 Illustration of marker placement for the direct joint centers (indicated by the circles, left side shown) along with the conventional full body marker set and the base of support markers. Green markers: shared with the conventional 39 marker set.

3.2 Study Design

In this protocol study, two motion conditions of distinct movement characteristics, (i.e., static vs. dynamic) were used to examine the fidelity of the two approaches. The first motion

condition is quiet standing, wherein participants adopted an upright standing posture with the elbow joints flexed 90 degrees to simulate a weight carrying posture. This condition allowed the analysis of static stability, providing baseline accuracy of the two approaches due to the least amount interference from body motion. Additionally, the center of pressure (CoP) was tracked using a force plate the participants were standing on. Since the CoP is the vertical projection of the CoM in static conditions, it provided a means to validate the accuracy of CoM calculated from the motion data. The second motion condition was walking on a level surface. This condition allowed the analysis of dynamic stability, thus revealing the robustness of the two approaches under the interference of body motion and other potential issues in motion capture (e.g., marker blockage). Particularly, the subjects were asked to walk at their chosen speed for 5 steps, starting and ending with a standing posture with two feet placed side-by-side.

Under each motion condition, three weight carrying tasks were performed, including holding a weight carrying posture with empty hands, carrying weight (barbells with handles, 7.0 kg) in hands, and carrying weight in hands and wearing a mock exoskeleton (a vest with barbells attached to the vest, 10.3 kg in total). This exoskeleton was designed for the slip and fall study, it consists of Mountaineering-Style Pad Set vest manufactured by Down East LLC Innovation. One inch squared aluminum rods was attached to the vest with the intention to hold the weight at the shoulder level. To simulate the weight of the exoskeleton of this kind, the barbell around 7 kg was attached to the lower half of the vest (Figure 3.7). For safety, the hand weight, along with the exoskeleton weight, was lower than the NIOSH's weightlifting standards at the 23.13 kg limit. The weight carrying posture was defined as both elbow joints flexing 90 degrees and the feet at the shoulder width apart. These three tasks, with increased difficulties in balance control, allowed the examination of the exoskeleton effect more precisely.

Therefore, there are 6 testing conditions in total in this study as the combinations of the body motion (2 levels) and the tasks (3 levels). During the quiet standing condition, the participants stood quietly for 30 seconds while the whole-body kinematics and the ground reaction force data were recorded. Each task condition during quiet standing was repeated 3 times. During the walking condition, the whole-body kinematics were recorded (the force plate data were recorded but not analyzed in this thesis work). Each task condition during walking was repeated 5 times.

3.2.1 Randomization of testing sequence

The three weight carrying tasks were permuted using a Latin square – Williams design that generated 6 task sequences. Each participant adopted one testing sequence. The two motion conditions were not randomized with the participants starting with quiet stand followed by walking.

3.3 Experimental Procedures

3.3.1 Subjects

Data from 4 healthy male subjects with a mean age at 32.8±13.5 years old, a mean height at 1.73±0.07 m, and a mean body mass at 70.2±9.7 kg were analyzed in this thesis work. The informed consent process was administered to all subjects. Signatures on the consent document were obtained prior to enrollment. The research was conducted at the NIU main campus, DeKalb, IL. The NIU IRB approval number of this thesis work is HS23-0156.

3.3.2 Inclusion and Exclusion Criteria

Subjects were included in the study if they were healthy and between the ages of 18 and 60 years and had no history of spinal deformity or other spinal ailment. Subjects were excluded if they had a history of major upper and lower extremity injury, a previous injury that may affect gait.

3.3.3 Experimental Setup

There were two motion conditions and three task conditions tested in the experiment. Figure 3.4 demonstrates the empty hand testing conditions during quiet standing and walking with elbows flexing 90 degrees to pretend weight carrying. Figure 3.5 demonstrates the weight carrying tasks during quiet standing and walking. Figure 3.6 demonstrates the weight carrying tasks while wearing the mock exoskeleton during quiet standing and walking. Particularly during walking, the participants walked on a platform and landed only one foot on one force plate during walking

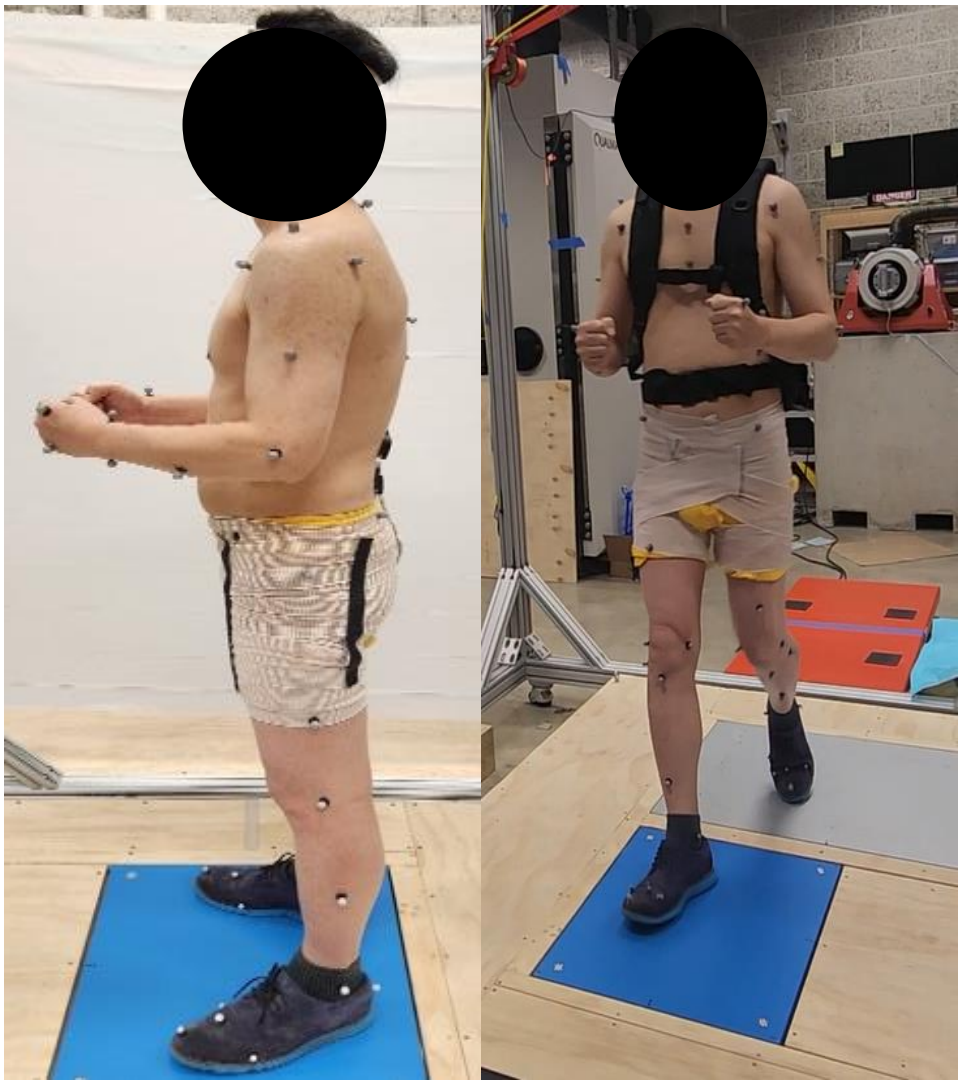

Figure 3.4 Illustration of quiet standing and walking with empty hands.

Figure 3.5 Illustration of quiet standing and walking conditions with weight in hands.

Figure 3.6 Illustration of quiet standing and walking conditions with weight in hands while wearing a mock exoskeleton.

The hand weight CoM and the exoskeleton CoM were tracked with markers placed on them and subsequently used for the whole-body CoM calculation. Figure 3.7 shows the marker placement on the hand weight and the mock exoskeleton for tracking their CoM. Two extra markers were placed on the mock exoskeleton to mimic the T10 and RBAK markers such that

the Motive software could auto-label the markers used in the conventional full-body marker set. However, these two markers on the exoskeleton were not used in the CoM computation. The determination of the CoM of the hand weight was determined by the CoM (i.e., the geometric center) of two weight components. The structure of the mock exoskeleton was complex. Its CoM was determined by handing the exoskeleton in two orientations using a cable. A marker was placed on the cable. The CoM was aligned with the vertical direction of the marker. Therefore, the interaction of two vertical lines obtained in two hanging positions determined the CoM of the exoskeleton. The relations between the markers placed on the hand weight and the mock exoskeleton and their CoM were then obtained and subsequently used in tests to track their movements.

3.4 Data Collection and Processing

In the present study, a 3D optical motion capture system with 8 cameras (Flex 13, NaturalPoint, Inc. Corvallis, OR) and the companying Motive 2.3.5 software was used for the whole-body kinematic data collection at a sampling rate of 120 Hz. The Motive software was also used for motion data cleaning such filling gaps. If the marker data had problems such as too large gaps and erroneous behavior and not repairable, the data were excluded from further CoM analysis. The biomechanical analysis software Visual3D (C-motion, Inc., Germantown, MD) was used for the creation of the skeleton model and calculations of joint centers and CoM for each segment and the whole-body CoM. The whole-body CoM was computed in 4 methods from the

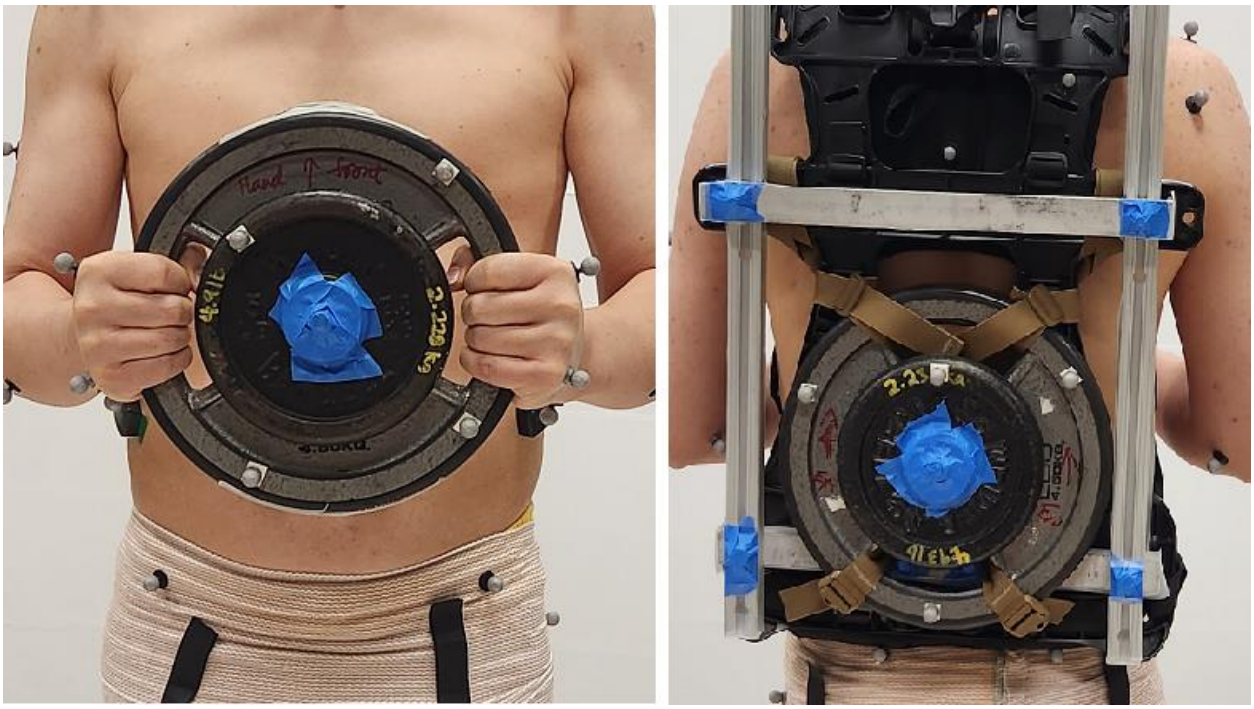

Figure 3.7 The marker placement for the hand weight (left, 4 markers) and the mock exoskeleton (right, 4 markers on the weight and 2 markers on the vest).

motion capture data: 1) directly from the marker data (RawJC), 2) from the skeletal model-produced joint center (ModelJC), 3) from the model-produced CoM (ModelCoM), and 4) the model-directly produced CoM (ModelWB). Additionally, CoP was obtained using the force plate (FPCoP) during quiet standing and served as the golden standard for comparison of with the motion data derived CoM.

The ground reaction forces were obtained using a force plate (9287CA, Kistler Instrument Corp., Novi, MI) at a sampling rate of 1000 Hz. The force plate data were collected using a custom-written LabVIEW program (National Instrument Inc., Austin, TX). The CoP was computed from the ground reaction force data. A low-pass filter with cut-off frequency at 6 Hz was applied to smooth the CoP time-series data and the CoM time-series data obtained using motion capture data.

3.4.1 Direct Joint Center Determination

The joint centers were determined directly from associated markers as shown in Table 3.4. The CoM defined in the Dempster segmentation method was used to determine segmental CoM except the HNT, hand, and foot segments (described in the Section 3.1.1). Finally, the whole-body CoM (RawJC CoM) was readily calculated based on the segmental CoM and segmental masses. Particularly, a cubic interpolation method (MATLAB spline function) was used to calculate the segmental mass based on the body mass.

Table 3.4 The creation of joint centers in the direct center of joint approach.

Joint Center (left side shown)	**Starting marker**	**Ending marker**	**Offset ML/AP/Axial**
Shoulder	LSF	LSB	Axial – 0.5
Elbow	LELB	LHME	Axial – 0.5
Wrist	LWRA	LWRB	Axial – 0.5
Hip	LP	RP	Axial – 0.25
Knee	LKNE	LIKNEE	Axial – 0.5
Ankle	LANK	LIANKLE	Axial – 0.5

3.4.2 The Skeleton Model-Generated CoM Using Three Methods

The skeleton model predicts the proximal and distal ends of segments based on a set of algorithms specific to each segment (Table 3.5). The landmark values for creating CoM for each segment are shown in Table 3.6. Each participant had his own skeleton model created based on individual height and body mass. It is noteworthy that the T10 and RBAK markers on the back were blocked by the mock exoskeleton during the weight carrying while wearing exoskeleton task. While two extra markers were placed on the mock exoskeleton, they were only used for the auto-labeling purpose in the Motive software. During the model creation in the Visual3D, the Thorax_Dist landmark were created using the C7, CLAV, and STRN markers assuming a rigid thorax.

Table 3.5 The landmark values for creating joint centers in the skeletal model.

Joint Center	Starting	End	Lateral Object	Reference Segment	Offset ML/AP/Axial
Head_Front	LFHD	RFHD			Axial – 0.5
Head_Back	LBHD	RBHD			Axial – 0.5
Head_Mid	Head_Front	Head_Back	-	-	Axial – 0.5
Thorax_Prox	CLAV	C7	-	-	Axial – 0.5
Thorax_Dist	STRN	T10	-	-	Axial – 0.5
Shoulder (LSJC)	LSHO	-		Thorax/Ab (frame)	Axial – (LShoulderRadius + MarkerRadius)
Elbow (LEJC)	LELB	LSJC	LWJC	-	ML - (LElbowRadius + MarkerRadius)
Wrist (LWJC)	LWRA	LWRB	-	-	Axial – 0.5
Left_Hip	LASI	-	-	Pelvis (frame)	ML – 0.36*ASIS_Distance* RPV_ML_Direction
					AP – 0.19*ASIS_Distance* RPV_AP_Direction
					Axial – 0.30*ASIS_Distance* RPV_Axial_Direction
Knee (LKJC)			-	Thigh	Axial – 1
Ankle (LAJC)			-	Shank	Axial – 1

Table 3.6 The landmark values for creating center of mass in the skeletal model.

CoM (left side shown)	Proxial End	Distal End	Offset ML/AP/Axial
Head	Head_Front	Head_Mid	Axial – 1
Thorax/Abd	Thorax_ Prox	Thorax_Dist	Axial – 0.505
Pelvis	MidASIS	MidPSIS (L5S1)	Axial – 0.5
Upper Arm	LSJC	LEJC	Axial – 0.3916
Forearm	LEJC	LWJC	Axial – 0.5235
Hand	LWJC	LFIN	Axial – 1
Thigh	LEFT_HIP	LKJC	Axial – 0.43985
Shank	LKJC	LAJC	Axial – 0.4557
Foot	LHEE	LTOE	Axial – 0.5

The skeletal model produced three levels of outcomes: 1) the model-produced joint centers, 2) the model-produced CoM, and 3) the model-produced whole-body CoM. The ModelJC CoM was calculated similar to the RawJC method by using the model-produced joint centers, the Dempster (1955) CoM (except the HNP segment), and the segmental masses defined in the work by Webb Associates (1978). Because the skeletal model separated the HNP segment into three segments, the model-produced CoM of these three segments were used instead. The ModelCoM CoM was calculated using the model-produced CoM and the segmental masses defined in the work by Webb Associates (1978).

3.5 Statistical Analysis

The IBM SPSS statistical software package (Version 28.0, IBM, Armonk, NY) was used to conduct data analysis. The descriptive data are shown as mean and standard deviation (SD). A mixed model analysis was used to determine the main effects of tasks and CoM computation methods on CoM data. The Bonferroni adjustment was used in post hoc test when the main factor analysis was significant. A $p<0.05$ indicates statistical significance.

Specifically for the quiet standing tests, the X (anterior-posterior – AP) and the Y (side-to-side) data were extracted from the 4 motion data-derived CoM data to form the motion data-derived CoP data and were compared together with the force plate-derived CoP data. For more meaningful comparisons between the CoP data, all data were treated by centering around (subtracting) the midpoint between the right and left ankle joint centers obtained from the motion data. The Z values of the CoM data were compared among the 4 CoM computation methods.

For the walking tests, there is no gold standard CoM to compare with. Therefore, in addition to compare between the mean CoM data over time of 4 CoM computing methods,

relative distance between the CoM obtained from difference methods were obtained. Here, the CoM obtained from the RawJC method was used as reference (subtracting). thus allowing better comparisons of three model-derived CoM data.

CHAPTER 4: RESULTS AND DISCUSSION

4.1 Whole-body Center of Mass during Quiet Standing

In this thesis work, the whole-body CoM was calculated using 4 methods from the motion capture data: 1) directly from the marker data (RawJC) without modeling, 2) from the skeletal model-produced joint center (ModelJC), 3) from the model-produced CoM (ModelCoM), and 4) the model-directly produced CoM (ModelWBCoM). Additionally, the CoP data were obtained using a force plate (FPCoP) during quiet standing and served as the golden standard for comparison with the motion data-derived CoP. Figure 4.1 shows CoP calculated from 4 motion data-based methods and from the force plate data for all quiet standing trials. To better compare between CoP computed using different methods, the results were re-centered around the midpoint between the right and left ankle joint centers and analyzed.

Figure 4.2 shows the descriptive results of the re-centered mean CoP (i.e., sway center) in the AP and SS directions. The main factor analyses showed a significant effect of the task factor on the sway center in the AP direction ($p<0.01$) but not in the SS direction ($p=0.34$). The post hoc analyses (Table 4.1) showed that the empty hands condition caused the sway center to move more anteriorly (~ 6 mm) than the other two conditions. There were significant effects of the CoP computing factor on the sway center in both the AP direction ($p<0.001$) and the SS direction ($p<0.001$). The post hoc analyses (Table 4.2) showed that the force plate-derived sway center located more posteriorly than the RawJC sway center (~ 18 mm) and the 3 model-produced sway centers (~ 40 mm to 45 mm). The RawJC sway center also located more posteriorly than the 3 model-produced sway centers (~ 21 mm to 26 mm). There was no statistical difference between the 3 model-derived sway centers. For the sway centers in the SS direction, the post hoc analyses

(Table 4.3) showed that the 4 motion data-derived sway centers were significantly to the left side of the midpoint between the ankle joints (~ 9 mm to 13 mm), while the force plate-derived sway center was almost at the center.

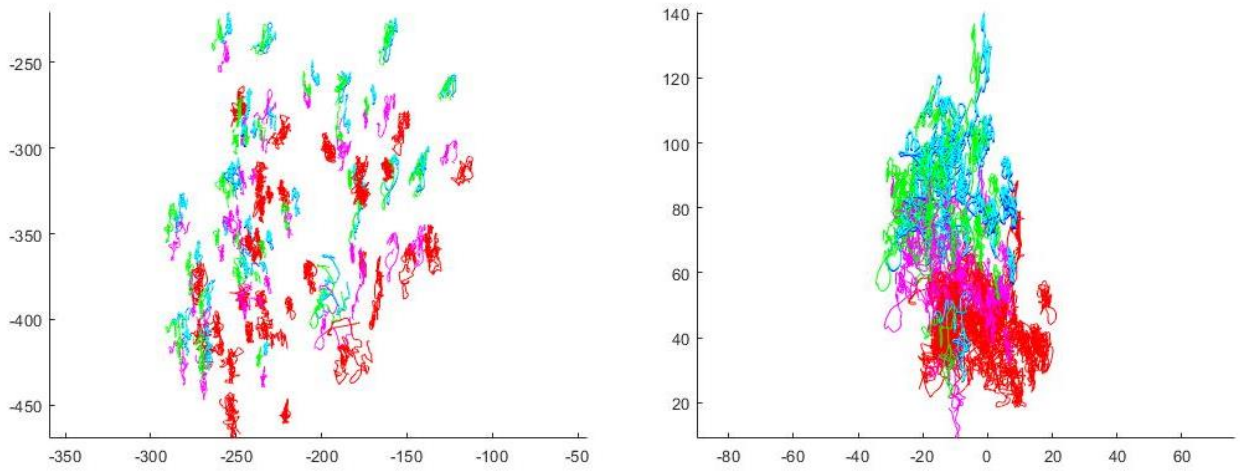

Figure 4.1 Postural sway (mm) calculated from 4 motion data-based methods and from the force plate. X axis – side-to-side direction, Y axis – anterior-posterior direction. All trials are ploted either in raw data (left) or re-centered by the midpoint between the right and left ankle joints (right). Red: force plate; magenta: RawJC; blue: ModelJC; cyan: ModelCoM; and green: ModelWBCoM.

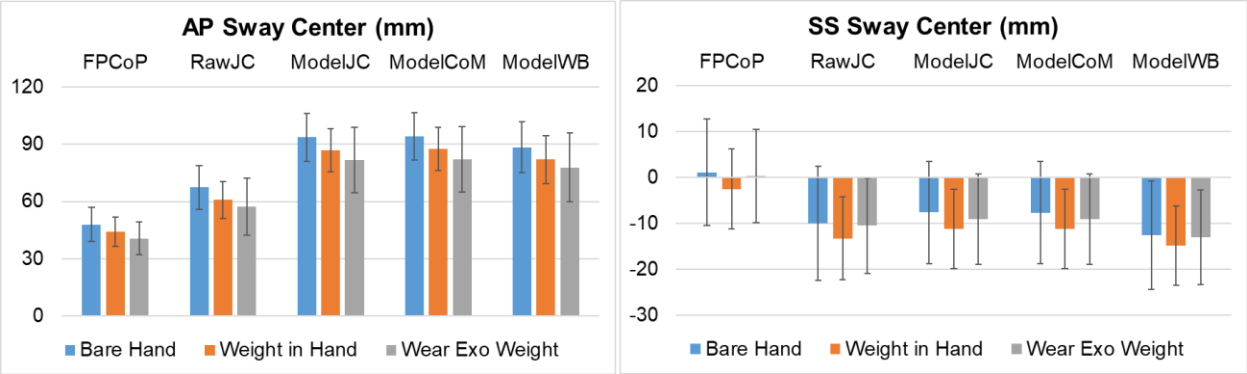

Figure 4.2 The mean and standard deviation of the sway center in the anterior-posterior (AP) direction and the side-to-side (SS) directions (re-centered).

Table 4.1 P values of the post hoc analyses of the task conditions on the sway center in the anterior-posterior direction (re-centered).

	Empty Hands	Weight in Hands	Wear Exoskeleton
Empty Hands	-	0.01	0.007
Weight in Hands	-	-	1
Wear Exoskeleton	-	-	-

Table 4.2 P values of the post hoc analyses of the 5 CoP computation methods on the sway center in the anterior-posterior direction (re-centered).

	FPCoP	RawJC	ModelJC	ModelCoM	ModelWBCoM
FPCoP	-	<0.001	<0.001	<0.001	<0.001
RawJC	-	-	<0.001	<0.001	<0.001
ModelJC	-	-	-	1	0.855
ModelCoM	--	--	-	-	0.558
ModelWBCoM	-	-	-	-	-

Table 4.3 P values of the post hoc analyses of the 5 CoP computation methods on the absolute sway center in the side-to-side direction (re-centered).

	FPCoP	RawJC	ModelJC	ModelCoM	ModelWBCoM
FPCoP	-	<0.001	<0.001	<0.001	<0.001
RawJC	-	-	<0.001	<0.001	<0.001
ModelJC	-	-	-	1	0.855
ModelCoM	--	--	-	-	0.558
ModelWBCoM	-	-	-	-	-

Figure 4.3 shows the descriptive results of the 90-percentile postural sway (from 5% to 95%) in the AP direction (AP Sway) and in the side-to-side direction (SS Sway) and the mean sway speed. The re-center procedure about the midpoint between the ankle joints had no effect on the AP sway or the SS sway as they were centered around the mean CoP in each testing trial. The main factor analyses showed significant effects of the CoP computing factor on the SS sway ($p<0.001$) and the sway speed ($p<0.001$). The post hoc analyses demonstrated significantly larger SS sway (Table 4.4) and faster sway speed (Table 4.5) in the force plate-derived CoP than the 4 motion data-derived CoP, while there was no difference between the 4 motion data-derived CoP. These observations may be in part attributed to the sampling rate difference: 1000 Hz for the force plate and 120 Hz for the motion capture. While not tested, there were larger variabilities in CoP under the hand weight task condition, even from the force plate-derived CoP. This observation may be an indication of difficulty in control body sway with weight in the hands.

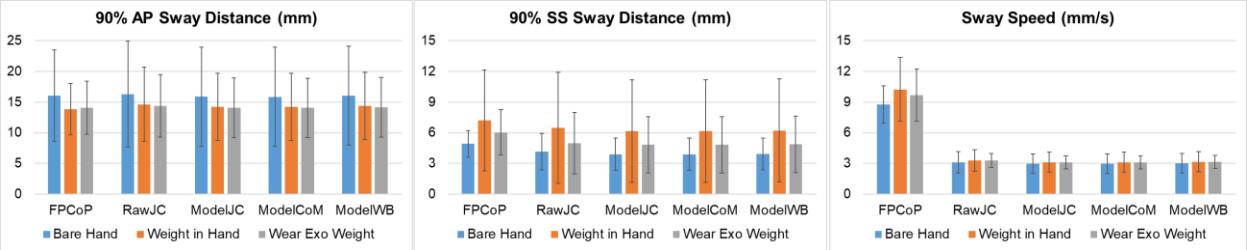

Figure 4.3 The mean and standard deviation of the postural sway in the anterior-posterior (AP) and side-to-side (SS) directions and the average sway speed.

Table 4.4 P values of the post hoc analyses of the CoP computation methods on the 90 percentile side-to-side sway range.

	FPCoP	RawJC	ModelJC	ModelCoM	ModelWBCoM
FPCoP	-	0.007	0.005	0.005	0.014
RawJC	-	-	1	1	1
ModelJC	-	-	-	1	1
ModelCoM	--	--	-	-	1
ModelWBCoM	-	-	-	-	-

Table 4.5 P values of the post hoc analyses of the CoP computation methods on the sway speed.

	FPCoP	RawJC	ModelJC	ModelCoM	ModelWBCoM
FPCoP	-	<0.001	<0.001	<0.001	<0.001
RawJC	-	-	0.901	0.887	1
ModelJC	-	-	-	1	1
ModelCoM	--	--	-	-	1
ModelWBCoM	-	-	-	-	-

Different from the force plate, the motion data also produced CoM in the vertical direction (Com-Z). The descriptive results of the CoM-Z are shown in Figure 4.4. There was a significant task effect ($p<0.01$) in CoM-Z. The post hoc test (Table 4.6) shows the CoM-Z was significantly higher in the exoskeleton task than the Com-Z in the empty hands task. This observation indicates that the exoskeleton weight shews the CoM in the vertical direction.

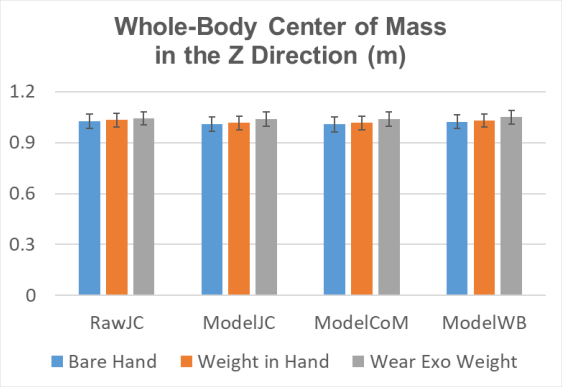

Figure 4.4 The mean and standard deviation of the CoM in the Z direction.

Table 4.6 P values of the post hoc analyses of the 4 CoM computation methods on the whole-body-CoM in the Z direction without force plate data.

	Empty Hands	Weight in Hands	Wear Exoskeleton
Empty Hands	-	1	0.006
Weight in Hands	-	-	0.071
Wear Exoskeleton	-	-	-

4.2 Whole-body Center of Mass during Walking

In the funded study, the CoM motion during simulated slip and fall is the primary interest. Therefore, the walking test was employed in this thesis work to determine the robustness of the different CoM computing methods under dynamic conditions. Figure 4.5 illustrates the movement of CoM over time in one walking trial as computed using 4 motion data-based methods: RawJC, ModelJC, ModelCoM, and ModelWBCoM. The CoM derived using these 4 methods were compared in two ways. First the mean CoM over time was compared to get the ballpark of the robustness (Figure 4.6). Second the differences between the CoM were compared with the RawJC as the reference (by subtracting RawJC CoM) (Figure 4.7), thus providing differential estimates of the robustness of three model-based methods.

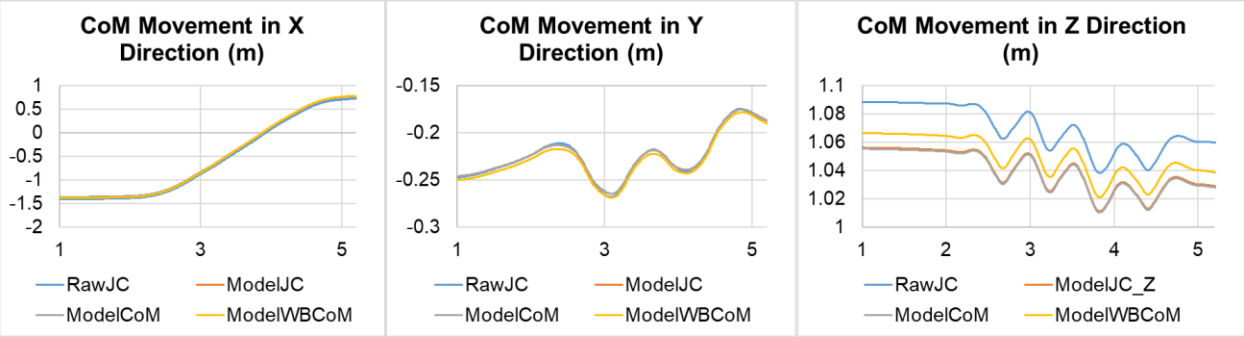

Figure 4.5 The movement of CoM over time during a walking trial as calculated using 4 motion data-based CoM computation methods.

Figure 4.6 The mean CoM over time during walking.

The mean CoM in the X (forward), Y (right-to-left) and Z (vertical) direction are shown in Figure 4.6. The main factor analyses showed significant effects in the task factor on mean CoM in the X direction ($p<0.01$) and the Z direction ($p<0.001$). Since there was no specific control during walking (e.g., the participants chose their own walking style), the interpretation of mean CoM-X and mean CoM-Y is not meaningful. However, the mean CoM-Z could reveal useful information as the ground level is same for all trials. The post hoc test (Table 4.7) on the mean CoM-Z showed that the mean Com-Z was significantly higher in the weight carrying with the exoskeleton tasks than the other two task conditions.

Table 4.7 P values of the post hoc analyses of the task conditions on the mean CoM over time in the Z direction.

	Empty Hands	Weight in Hands	Wear Exoskeleton
Empty Hands	-	0.361	<0.001
Weight in Hands	-	-	<0.001
Wear Exoskeleton	-	-	-

The descriptive results of the CoM difference in the X, Y, Z directions and the overall distance are presented in Figure 4.7. The main factor analyses showed significant effects in the task factor in all direction and the overall distance ($p<0.05$ in X, $p<0.001$ in Y and Z, and $p<0.01$ in overall distance) and in the CoM computing factor in the X ($p<0.01$), Y ($p<0.001$) and Z directions ($p<0.001$). The statistical significances in for the task factor were not meaningful because the subtractions were done between data processing methods (i.e., only meaningful to tell differences between data processing methods). The post hoc analyses for the CoM computing method factor are shown in Table 4.8 to Table 4.10. Compared to the other two methods, the ModelWBCom – RawJC values showed that the ModelWBCom-derived CoM was less anterior in the X direction (19.1 mm in ModelWBCom vs. 24 mm to 25 mm in the other two methods), a shift to the right side in the Y direction (-3.3 mm vs. 2.0 mm), and higher in the Z directions (1.2 mm vs. -12 mm to -13 mm), while no difference was found between ModelJC – RawJC and ModelCoM – ModelJC. Overall, the RawJC and the ModelWBCoM were similar in CoM computation while the ModelJC and ModelCoM methods were similar. Given that the RawJC method doesn't require any advanced digital human modeling or computing power, the RawJC method appears to be a viable choice for the particular application that uses whole-body CoM as the primary parameter for the risk of falls analysis.

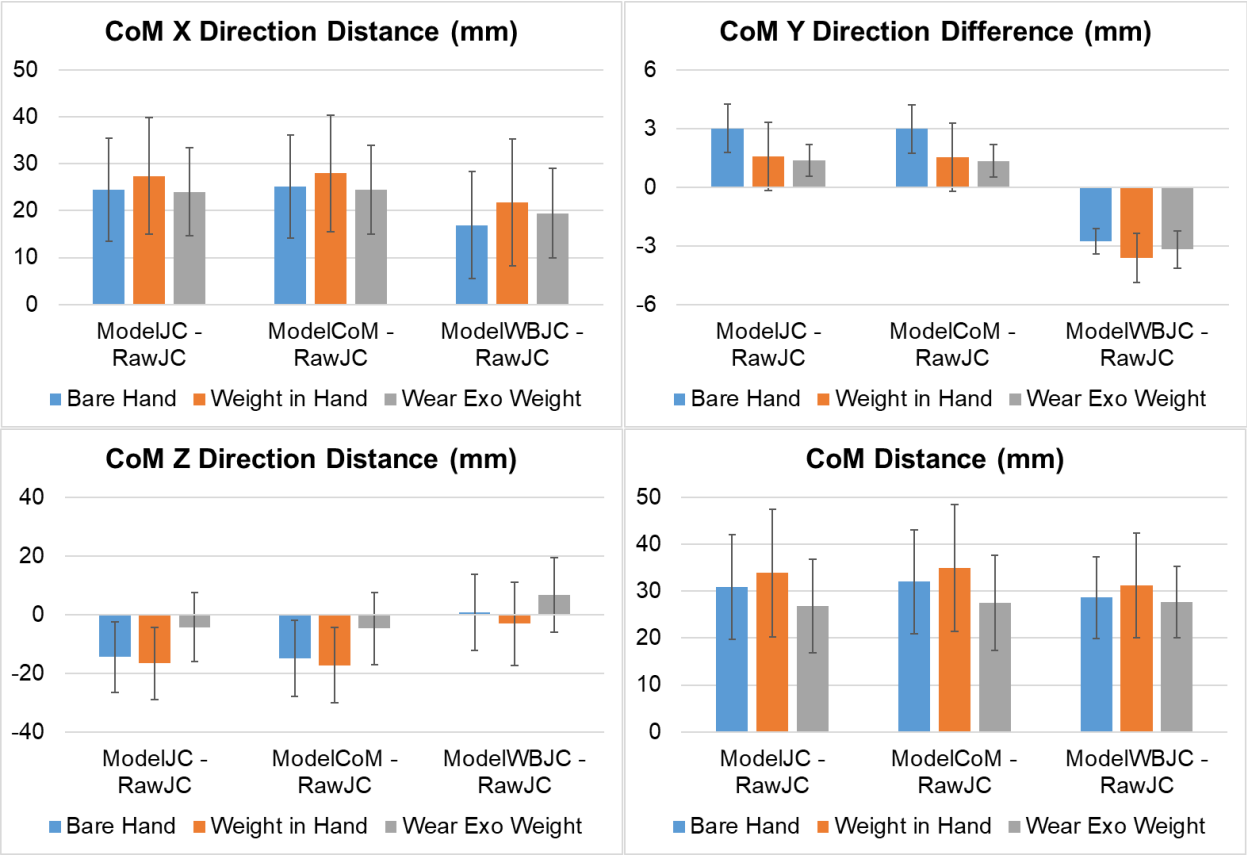

Figure 4.7 The mean CoM difference over time during walking between the model-produced CoM and the raw motion data derived CoM. Note: the empty hands task dataset analyzed using the ModelWBCoM is excluded.

Table 4.8 P values of the post hoc analyses of the CoM computation methods on mean CoM difference in the X direction.

	ModelJC – RawJC	MdoelCom – RawJC	ModelWBCom – RawJC
ModelJC – RawJC	-	1	0.015
MdoelCom – RawJC	-	-	0.006
ModelWBCom – RawJC	-	-	-

Table 4.9 P values of the post hoc analyses of the CoM computation methods on mean CoM difference in the Y direction.

	ModelJC – RawJC	MdoelCom – RawJC	ModelWBCom – RawJC
ModelJC – RawJC	-	1	<0.001
MdoelCom – RawJC	-	-	<0.001
ModelWBCom – RawJC	-	-	-

Table 4.10 P values of the post hoc analyses of the CoM computation methods on mean CoM difference in the Z direction.

	ModelJC – RawJC	MdoelCom – RawJC	ModelWBCom – RawJC
ModelJC – RawJC	-	1	<0.001
MdoelCom – RawJC	-	-	<0.001
ModelWBCom – RawJC	-	-	-

Together, the data collected in this thesis work suggest that both the RawJC and ModelWBCoM were suitable to study the risk of falls during slips and falls, with a slight preference to the RawJC method due to its simplicity.

4.3 Limitations

There are a few limitations presented in this thesis work. The sample size of 4 is small though justified for a protocol study. The data obtained from this study can be used to calculate the sample size of future studies. Ideally, the female subjects should be included as part of the

sample size. The female body shapes are different compared to the male body shapes. The results of this study may not be applicable for female subjects. Second, the walking condition used in this thesis work may not be dynamic enough when compared to the slip and fall events to be studied in the funded research. Third, the shoulder joint marker placement in the direct center of joint approach is sufficient for this thesis work due to limited motion in the shoulder joints. A large arm motion is expected during a falling event as an attempt to regain balance. It remains to be seen how well this shoulder joint marker placement performs during actual falling events. Last but not least, even if it is concluded that using the direct center of joint approach is reasonable for the funded study, the skeletal model-based approach can provide a lot more kinematic information such as joint orientation, velocity and acceleration, and etc. It is noteworthy in the funded research that the subject is holding cater in the hands, substantially block the markers (right and left ASIS) in front of the pelvis. In the direct center of joint approach, the markers are placed at the great trochanters thus avoid the marker blocking problem. Care needs to be taken when generalizing the study findings to other applications.

CHAPTER 5: CONCLUSIONS

This thesis work was part of a funded research aiming to determine the effects of exoskeleton use on balance control. The primary purpose of this thesis work was to determine a reliable maker placement protocol that will be used in the funded research. Two motion data-based approaches were chosen to track full-body kinematics – a direct center of joint approach and a skeletal model-based approach. The participants were asked to perform 3 tasks during quiet standing and during walking: 1) holding a weight carrying posture with empty hands, 2) carrying weight (7.0 kg) in the hands, and 3) carrying weight in the hands while wearing a mock exoskeleton (10.3 kg). During quiet standing, all four motion data-based methods were compared to the center of pressure (FPCoP) obtained using a force plate placed under the participant's feet. The results showed that the FPCoP was posterior to the RawJC-derived CoM, which was in turn posterior to the 3 model-derived CoM. In the side-to-side direction, the FPCoP located at the middle while the 4 motion data-based CoM were slightly to the left side. The anterior-posterior sway distance, the side-to-side sway distance and the sway speed analyses showed no difference between the 4 motion data-based methods. The task effect analyses showed that wearing the mock exoskeleton caused the CoM to shift a higher position. Also, carrying weight in hands and carrying weight while wearing an exoskeleton caused CoM to shift posteriorly. Both observations on the task effect indicate potentially compromised balance ability. During walking, the analyses of the CoM computing method effect showed that the RawJC and ModelWBCoM methods were similar while the ModelJC and ModelCoM were similar. Together, the data collected in this thesis work suggest that both the RawJC and ModelWBCoM were suitable to

study the risk of falls during slips and falls, with a slight preference to the RawJC method due to its simplicity.

REFERENCES

Anderson, J. A. (1984). Shoulder pain and tension neck and their relation to work. *Scandinavian Journal of Work, Environment & Health*, *10*(6), 435–442. https://doi.org/10.5271/sjweh.2300

Burkhart, K., Grindle, D., Bouxsein, M. L., & Anderson, D. E. (2020b). Between-session reliability of subject-specific musculoskeletal models of the spine derived from optoelectronic motion capture data. *Journal of Biomechanics, 112,* 110044. https://doi.org/10.1016/j.jbiomech.2020.110044

Cheng, H., Obergefell, L., & Rizer, A. (1994). *Generator of body (GEBOD) manual*. Armstrong Laboratory, Air Force Material Command.

Dempster, W. T., *Space Requirements of the Seated Operator,* WADC-TR-55-159, Aerospace Medical Research Laboratories, Dayton, Ohio, 1955.

Grooten, W. J., Billsten, E., von Stedingk, S., & Reimeringer, M. (2022). Biomechanical analysis of lifting on stable versus unstable surfaces—a laboratory-based proof-of-concept study. *Pilot and Feasibility Studies*, *8*(1). https://doi.org/10.1186/s40814-022-01157-2

Haddas, R., Ju, K. L., Boah, A., Kosztowski, T., & Derman, P. B. (2019). The effect of surgical decompression on functional balance testing in patients with cervical spondylotic myelopathy. *Clinical Spine Surgery: A Spine Publication*, *32*(9), 369–376. https://doi.org/10.1097/bsd.0000000000000889

Haddas, R., Kosztowski, T., Mar, D., Boah, A., & Lieberman, I. (2021a). Balance effort, cone of economy, and dynamic compensatory mechanisms in common degenerative spinal pathologies. *Gait & Posture*, *89*, 67–73. https://doi.org/10.1016/j.gaitpost.2021.04.038

Haddas, R., Wood, A., Lieberman, I., & Derman, P. B. (2021). Assessing the cone of economy in patients with spinal disease using only a force plate: An observational retrospective cohort study. *European Spine Journal*, *30*(9), 2504–2513. https://doi.org/10.1007/s00586-021-06836-x

Kim, S., Nussbaum, M. A., Esfahani, M. I. M., Alemi, M. M., Alabdulkarim, S., & Rashedi, E. (2018). Assessing the influence of a passive, upper extremity exoskeletal vest for tasks requiring arm elevation: Part I– "Expected" effects on discomfort, shoulder muscle activity, and work task performance. Applied ergonomics, 70, 315-322.

Kudernatsch, S., & Peterson, D. R. (2018). Biomechanical Testing of an Upper-Extremity Occupational Exoskeleton-Preliminary Report on Methodologies and Pilot Data. In Proceedings of the Human Factors and Ergonomics Society Annual Meeting (Vol. 62, No. 1, pp. 2013-2017). Sage CA: Los Angeles, CA: SAGE Publications.

Lowe, B. D., Billotte, W. G., & Peterson, D. R. (2019). ASTM F48 Formation and Standards for Industrial Exoskeletons and Exosuits. IISE Transactions on Occupational Ergonomics and Human Factors, (just-accepted), 1-8.

Miller D.I., and R.C. Nelson. 1973. Biomechanics of Sport. Philadelphia: Lea & Febiger. Plagenhoef, S. 1971. Patterns of Human Motion: A Cinematographic Analysis. Englewood Cliffs, NJ: Prentice Hall.

Rakshit, R., Xiang, Y., & Yang, J. (2020). Dynamic-joint-strength-based two-dimensional symmetric maximum weight-lifting simulation: Model development and validation. *Proceedings of the Institution of Mechanical Engineers, Part H: Journal of Engineering in Medicine, 234*(7), 660–673. https://doi.org/10.1177/0954411920913374

U.S. Bureau of Labor Statistics. (2018). Occupational injuries and illnesses resulting in musculoskeletal disorders (MSDs). Retrieved September 8, 2023, from https://www.bls.gov/iif/factsheets/msds.htm

Webb Associates, *Anthropometric Source Book, Vol. 1, NASA 1024,* National Aeronautics and Space Administration, Washington, DC, 1978.

Winter, D.A. 1990. Biomechanics and Motor Control of Human Movement. 2nd ed. Toronto: Wiley.